Comparison of simulated neutrino emission models with data on Supernova 1987A

Jackson Olsen⬤ and Yong-Zhong Qian⬤

School of Physics and Astronomy, University of Minnesota, Minneapolis, Minnesota 55455, USA

We compare models of supernova (SN) neutrino emission with the Kamiokande II data on SN 1987A using the Bayesian approach. These models are taken from simulations and are representative of current one-dimensional SN models. We find that models with a brief accretion phase of neutrino emission are the most favored. This result is not affected by varying the overall flux normalization or considering neutrino oscillations. We also check the compatibility of the best-fit models with the data.

I. INTRODUCTION

In this paper, we compare neutrino emission models representative of current one-dimensional (1D) supernova (SN) simulations with the data on SN 1987A. Approximately 20 neutrino events were observed by the Kamiokande II (KII) [1,2], Irvine-Michigan-Brookhaven (IMB) [3], and Baksan [4] detectors. These events have been extensively studied to understand SN neutrino emission and neutrino properties (see, e.g., [5] for a review of earlier works and, e.g., [6,7] for detailed methodical analyses). The common practice was to use parametric models of SN neutrino emission and extract several parameters from the relatively sparse data for comparison with the results from SN neutrino transport calculations. These calculations have been greatly refined over the past several decades, during which there have been major advances in SN modeling (see, e.g., [8,9] for reviews). Rather than approximating these detailed SN neutrino emission models with some simplified parametrization, it is interesting to compare them directly with the SN 1987A data. We follow [6] and use the Bayesian approach for such comparisons in this paper. This approach provides a straightforward way to rank the models in light of the data. We also check the compatibility of the best-fit models with the data.

We take three baseline models from the Garching group [10]: z9.6-SFHo, s20-SFHo, and s27-LS220, which will be referred to as models A, B, and C, respectively. Models A and C were described in detail in [9]. These three models are representative of current 1D SN simulations and cover a range of neutrino emission for comparison with the SN 1987A data. We also vary the overall flux normalization to obtain models A′, B′, and C′ as counterparts of models A, B, and C and consider three cases of neutrino oscillations for each model. In total, we compare 18 models with the SN 1987A data from the KII detector. We focus on the 11

neutrino events observed in this detector because the IMB detector had issues of failing photomultiplier tubes [3] and, therefore, is harder to characterize while the Baksan detector reported significantly fewer events. We find that models with a brief accretion phase of neutrino emission are the most favored. This result is not affected by varying the overall flux normalization or considering neutrino oscillations.

This paper is organized as follows. We describe our adopted SN neutrino emission models in Sec. II and our Bayesian approach to compare them with the data in Sec. III. We present the results in Sec. IV and check the compatibility of the best-fit models with the data in Sec. V. We summarize our results and give conclusions in Sec. VI.

II. NEUTRINO EMISSION MODELS

In general, the neutrino emission relevant for comparison with the SN 1987A data consists of an accretion phase followed by a much longer cooling phase. During the accretion phase, material is still falling through the standing SN shock onto the proto-neutron star (PNS) and the release of the gravitational binding energy of this material gives rise to enhanced emission of ν_e and $\bar{\nu}_e$ over ν_x and $\bar{\nu}_x$ ($x = \mu, \tau$) through $e^- + p \to n + \nu_e$ and $e^+ + n \to p + \bar{\nu}_e$. The duration of this phase depends on the details of the explosion. It is brief for a light progenitor such as the one of 9.6 $M_\odot$ in model A, where the density of the infalling material rapidly decreases with the radius and consequently the shock experiences only a little hindrance in moving out. In contrast, the shock has a much harder time overcoming the infalling material in more massive progenitors such as those of 20 and 27 $M_\odot$ in models B and C, respectively, and, therefore, there are extended accretion phases of neutrino emission in these models. For all cases with a stable PNS, most of the gravitational binding energy is carried away during the cooling phase, when all neutrino

species have approximately the same luminosity. The gravitational binding energy of the PNS depends on both the progenitor and the nuclear equation of state (EoS). The SFHo EoS from [11] was used for models A and B, and the LS220 EoS from [12] with a compression modulus of 220 MeV was used for model C.

In the absence of flavor oscillations, the energy-differential number flux of a neutrino species ν_β at a distance d from its SN source is

$$F_{\nu_\beta}(E_\nu, t) = \frac{L_{\nu_\beta}}{4\pi d^2 \langle E_{\nu_\beta} \rangle} f_{\nu_\beta}(E_\nu, t), \qquad (1)$$

where L_{ν_β} and $\langle E_{\nu_\beta} \rangle$ are the ν_β luminosity and average energy, respectively, and $f_{\nu_\beta}(E_\nu, t)$ is the normalized ν_β energy spectrum. This spectrum can be fitted to the form (e.g., [13])

$$f_{\nu_\beta}(E_\nu, t) = \frac{T_{\nu_\beta}^{-1}(t)}{\Gamma(1 + \alpha_{\nu_\beta}(t))} \left(\frac{E_\nu}{T_{\nu_\beta}(t)} \right)^{\alpha_{\nu_\beta}(t)} e^{-E_\nu/T_{\nu_\beta}(t)}, \qquad (2)$$

where $\Gamma(1 + \alpha_{\nu_\beta})$ refers to the Gamma function, and α_{ν_β} and T_{ν_β} are related to the first and second moments of E_ν for the ν_β spectrum from SN simulations by

$$\alpha_{\nu_\beta} = \frac{2\langle E_{\nu_\beta} \rangle^2 - \langle E_{\nu_\beta}^2 \rangle}{\langle E_{\nu_\beta}^2 \rangle - \langle E_{\nu_\beta} \rangle^2} \qquad (3)$$

and

$$T_{\nu_\beta} = \frac{\langle E_{\nu_\beta} \rangle}{1 + \alpha_{\nu_\beta}}. \qquad (4)$$

Note that L_{ν_β}, $\langle E_{\nu_\beta} \rangle$, $\langle E_{\nu_\beta}^2 \rangle$, α_{ν_β}, and T_{ν_β} are functions of time, although we usually suppress their time dependence for convenience.

Because the SN neutrino events in the KII detector were induced predominantly by $\bar{\nu}_e$, we show in Fig. 1 the time evolution of $L_{\bar{\nu}_e}$, $\langle E_{\bar{\nu}_e} \rangle$, and $\alpha_{\bar{\nu}_e}$ for models A, B, and C. We also show the same information on $\bar{\nu}_x$ for consideration of neutrino oscillations. A duration of 13.5 s is chosen for comparison with the SN 1987A data. It can be seen from Fig. 1 that the turn-on of neutrino emission is extremely rapid for all models. We focus on the emission features subsequent to the turn-on below.

As mentioned above, models B and C have much more extended accretion phases (with significant excess of $L_{\bar{\nu}_e}$ over $L_{\bar{\nu}_x}$) than model A. The former two models also have higher $L_{\bar{\nu}_e}$ and $L_{\bar{\nu}_x}$ than the latter. The total energy $\mathcal{E}_\nu$ emitted in all neutrino species for each model is given in Table I. For all the models, $\langle E_{\bar{\nu}_e} \rangle$ and $\langle E_{\bar{\nu}_x} \rangle$ have some differences for the first ~ 1 s but are nearly the same later on. The difference between $\alpha_{\bar{\nu}_e}$ and $\alpha_{\bar{\nu}_x}$ persists at least up to
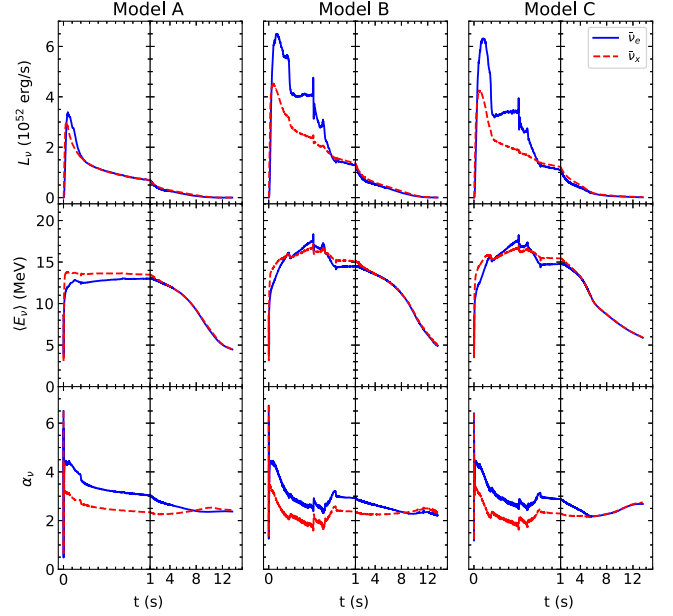

FIG. 1. The luminosity L_ν, average energy $\langle E_\nu \rangle$, and spectral parameter α_ν are shown as functions of time for $\bar{\nu}_e$ and $\bar{\nu}_x$ for the baseline models A, B, and C. Note the change of the time scale at $t = 1$ s.

$t \sim 5$ s but also diminishes at late times. In addition, the $\langle E_{\bar{\nu}_e} \rangle$ and $\langle E_{\bar{\nu}_x} \rangle$ for model B are significantly larger than those for model A. Because these two models employ the same EoS, their $\langle E_{\bar{\nu}_e} \rangle$ and $\langle E_{\bar{\nu}_x} \rangle$ have nearly constant differences for most of the evolution shown in Fig. 1. For model C with a different EoS, its $\langle E_{\bar{\nu}_e} \rangle$ and $\langle E_{\bar{\nu}_x} \rangle$ are close to those for model B up to $t \sim 4$ s. Subsequently, compared to model B, the $\langle E_{\bar{\nu}_e} \rangle$ and $\langle E_{\bar{\nu}_x} \rangle$ for model C decrease more rapidly for a brief period and then decrease more slowly.

Models A, B, and C were calculated for three different progenitors and employ two different forms of EoS; we consider that they cover a range of neutrino emission relevant for the case of SN 1987A. To study models with additional freedom, we also consider models A', B', and C' with scaled fluxes

$$F'_{\nu_\beta}(E_\nu, t) = \frac{K L_{\nu_\beta}}{4\pi d_0^2 \langle E_{\nu_\beta} \rangle} f_{\nu_\beta}(E_\nu, t), \qquad (5)$$

where K is a scale factor and $d_0 = 51.4$ kpc is the central value of the measured distance to SN 1987A [14,15].

TABLE I. Baseline models.

Model	Progenitor mass ($M_\odot$)	EoS	$\mathcal{E}_\nu$ (10^{53} ergs)
A	9.6	SFHo	1.99
B	20	SFHo	4.28
C	27	LS220	3.30

The scale factor K is the same for all neutrino species and allows the total emitted neutrino energy $\mathcal{E}_\nu$ to vary.

The $\bar{\nu}_e$ flux at the detector is modified by flavor oscillations. We consider three cases to sample these effects. Specifically, for models A, B, and C, the detected $\bar{\nu}_e$ flux is taken to be

$$F_{\mathrm{det}}(E_\nu, t) = f F_{\bar{\nu}_e}(E_\nu, t) + (1-f) F_{\bar{\nu}_x}(E_\nu, t), \quad (6)$$

where the constant f specifies the degree of mixing between $\bar{\nu}_e$ and $\bar{\nu}_x$. The reference case of no oscillations (NO) corresponds to $f = 1$. The other two cases correspond to $f = 0.681$ or 0.022 for just Mikheyev-Smirnov-Wolfenstein flavor transformation with the normal (NH) or inverted (IH) neutrino mass hierarchy, respectively [16–18]. The same three cases are also considered for models A′, B′, and C′. So altogether we compare eighteen models of SN neutrino emission with the SN 1987A data. For convenience, we add (NO), (NH), or (IH) to label a model when neutrino oscillations are of concern. For example, model A (NO) denotes model A with no oscillations, and model A (NH) denotes model A including oscillations with the NH.

III. BAYESIAN APPROACH TO COMPARE MODELS WITH DATA

The KII detector consisted of 2.14 kton of water in its fiducial volume and observed the neutrinos from SN 1987A predominantly through the Cherenkov radiation of the e^+ produced by inverse beta decay (IBD) $\bar{\nu}_e + p \rightarrow n + e^+$. Below we assume that all the neutrino events were due to IBD. The expected energy-differential rate of events including both the signal and the background is

$$\frac{d^2N}{dtdE}(E, t) = B(E) + N_p \int F_{\mathrm{det}}(E_\nu, t) \sigma_{\mathrm{IBD}}(E_\nu)$$

$$\times \frac{\epsilon(E_e)}{\sigma_E \sqrt{2\pi}} \exp\left[-\frac{(E - E_e)^2}{2\sigma_E^2}\right] dE_\nu, \quad (7)$$

where $B(E)$ is the background rate at energy E taken from [6] but treated as in [7], N_p is the total number of free protons within the fiducial volume, $\sigma_{\mathrm{IBD}}(E_\nu)$ is the IBD cross section, $E_e = E_\nu - \Delta$ is the energy of the e^+ from the IBD reaction, $\Delta = 1.293$ MeV is the neutron-proton mass difference, and $\epsilon(E_e)$ is the detection efficiency taken from [6]. Because of smearing, an e^+ of energy E_e may be detected at energy E, the probability of which is approximated by a Gaussian distribution with a standard deviation $\sigma_E = \sqrt{(0.75 \text{ MeV})E_e}$ [19,20] in Eq. (7).

Table II lists the detection time t_{det} and the detected energy E for each of the 11 KII events with $E \geq 7.5$ MeV for SN 1987A. The energy cutoff is chosen so that the models and the data are compared only for $t \leq 13.5$ s (there

TABLE II. KII data for SN 1987A.

t_{det} [s]	E [MeV]
0	20.0
0.107	13.5
0.303	7.5
0.324	9.2
0.507	12.8
1.541	35.4
1.728	21.0
1.915	19.8
9.219	8.6
10.433	13.0
12.439	8.9

were four events below the cutoff during $t_{\mathrm{det}} = 17.641$–$23.814$ s [6]). The first event is defined by $t_{\mathrm{det}} = 0$. Because of the random nature of detection, there is a time offset t_{off} between the first event and the model time $t = 0$ (the time of travel from SN 1987A to the detector is the same for all the events, and therefore, can be ignored). So $t = t_{\mathrm{det}} + t_{\mathrm{off}}$.

For a specific model M_i with a set of parameters $\boldsymbol{\theta}$, the probability of an event being detected with energy E at time $t_{\mathrm{det}} = t - t_{\mathrm{off}}$ is

$$p(E, t|\boldsymbol{\theta}, M_i) = \frac{1}{\langle N \rangle} \frac{d^2N}{dtdE}, \quad (8)$$

where $d^2N/dtdE$ refers to the expected energy-differential rate of events for model M_i, and

$$\langle N \rangle = \int_0^{13.5 \text{ s}} dt \int_{7.5 \text{ MeV}}^\infty dE \frac{d^2N}{dtdE} \quad (9)$$

is the expected total number of events. The likelihood of detecting a particular configuration of $N = 11$ events is

$$p(D|\boldsymbol{\theta}, M_i) = \frac{\langle N \rangle^N e^{-\langle N \rangle}}{N!} \prod_{j=1}^N p(E_j, t_j|\boldsymbol{\theta}, M_i), \quad (10)$$

where D represents the set of detection data, and E_j and t_j correspond to E and t for the jth event. The likelihood in Eq. (10) follows from the extended maximum likelihood method [21].

For all the models, the time offset t_{off} is a parameter. The other parameter is the distance d to SN 1987A for models A, B, and C or the scale factor K for models A′, B′, and C′. Our simple treatment of neutrino oscillations does not introduce any new parameters. In the Bayesian approach, the posterior probability for the parameters of model M_i is

$$p(\boldsymbol{\theta}|D, M_i) = \frac{p(D|\boldsymbol{\theta}, M_i) p(\boldsymbol{\theta}|M_i)}{p(D|M_i)}, \quad (11)$$

where $p(\boldsymbol{\theta}|M_i)$ is the prior probability for the parameters and

$$p(D|M_i) = \int p(D|\boldsymbol{\theta}, M_i)p(\boldsymbol{\theta}|M_i)d\boldsymbol{\theta}. \quad (12)$$

The prior probability $p(\boldsymbol{\theta}|M_i)$ is $p(d|M_i)p(t_{\text{off}}|M_i)$ or $p(K|M_i)p(t_{\text{off}}|M_i)$. We take $p(d|M_i)$ to be a Gaussian distribution with a mean of 51.4 kpc and a standard deviation of 1.2 kpc based on the measurement in [15], and we adopt uniform distributions for $p(t_{\text{off}}|M_i)$ and $p(K|M_i)$.

The Bayesian approach can also be applied to obtain the (discrete) posterior probability for model M_i as

$$p(M_i|D) = \frac{p(D|M_i)p(M_i)}{p(D)}, \quad (13)$$

where $p(M_i)$ is the prior probability for model M_i and

$$p(D) = \sum_i p(D|M_i)p(M_i). \quad (14)$$

Including three cases of neutrino oscillations, we take $p(M_i) = 1/9$ and consider the set of models A, B, and C separately from the set of their counterparts A′, B′, and C′. For comparing models M_i and M_j in a set, it is convenient to introduce the Bayes factor

$$B_{ij} = p(D|M_i)/p(D|M_j), \quad (15)$$

which is numerically the same as $p(M_i|D)/p(M_j|D)$ in our case. For $B_{ij} = 1-3$, $3-20$, $20-150$, and > 150, the evidence in favor of model M_i over model M_j is hardly noticeable, positive, strong, and very strong, respectively [6].

IV. RESULTS FROM BAYESIAN APPROACH

Using the posterior probability in Eq. (11), we calculate the best-fit values and the 68% and 95% credible regions for the parameters. These results are shown in Table III (IV) and Fig. 2 (Fig. 3) for models A, B, and C (A′, B′, and C′) including three cases of neutrino oscillations. Tables III and IV also give the expected total number of events $\langle N \rangle$ corresponding to the best-fit parameters and the posterior probability $p(M_i|D)$ [see Eq. (13)] for each model.

For models A, B, and C, because we have used the prior probability $p(d|M_i)$ based on the distance measurement, the best-fit values of d are essentially the same as the measured central value of 51.4 kpc regardless of neutrino oscillations. In addition, from the rapid turn-on of the neutrino luminosities (see Fig. 1), we expect little offset between the start of neutrino emission and the detection of the first $\bar{\nu}_e$ event, which is confirmed by the small best-fit values of $t_{\text{off}} = 0.024$–0.054 s for these models. On the other hand, the 95% credible regions enclose variations of $\sim \pm 1$ kpc in d ($\sim \pm 1\sigma$ measurement error) and values of

TABLE III. Best-fit values of d and t_{off} and the corresponding $\langle N \rangle$ for models A, B, and C including three cases of neutrino oscillations, along with the posterior probability for each model.

Model	d [kpc]	t_{off} [s]	$\langle N \rangle$	$p(M_i|D)$
A (NO)	51.39	0.048	6.81	0.2807
A (NH)	51.39	0.036	7.17	0.2684
A (IH)	51.39	0.024	7.92	0.2037
B (NO)	51.45	0.054	19.5	0.0058
B (NH)	51.45	0.054	19.4	0.0060
B (IH)	51.45	0.026	19.3	0.0043
C (NO)	51.43	0.051	15.1	0.0913
C (NH)	51.43	0.051	15.1	0.0875
C (IH)	51.43	0.033	15.0	0.0523

TABLE IV. Best-fit values of K and t_{off} and the corresponding $\langle N \rangle$ and p value for models A′, B′, and C′ including three cases of neutrino oscillations, along with the posterior probability for each model.

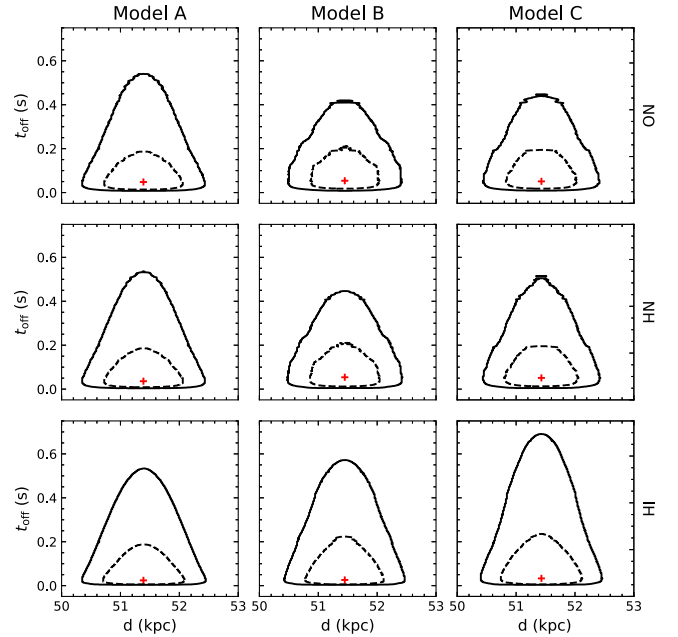| Model	K	t_{off} [s]	$\langle N \rangle$	p value	$p(M_i|D)$
A′ (NO)	1.32	0.048	8.90	0.16	0.2638
A′ (NH)	1.26	0.036	8.96	0.19	0.2223
A′ (IH)	1.15	0.024	9.06	0.25	0.1359
B′ (NO)	0.46	0.054	9.14	0.19	0.0400
B′ (NH)	0.47	0.054	9.29	0.25	0.0385
B′ (IH)	0.47	0.026	9.21	0.39	0.0245
C′ (NO)	0.60	0.051	9.18	0.12	0.1108
C′ (NH)	0.60	0.051	9.16	0.17	0.1038
C′ (IH)	0.61	0.033	9.27	0.25	0.0603

FIG. 2. The best-fit values (plus) and the 68% (dashed curve) and 95% (solid curve) credible regions for d and t_{off} are shown for models A, B, and C including three cases of neutrino oscillations.
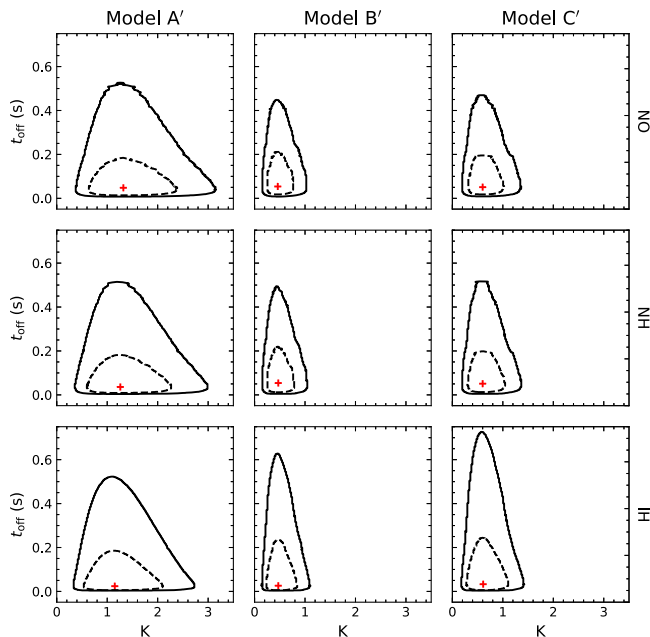
FIG. 3. The best-fit values (plus) and the 68% (dashed curve) and 95% (solid curve) credible regions for K and t_{off} are shown for models A′, B′, and C′ including three cases of neutrino oscillations.

t_{off} as large as 0.42 s for model B (NO) to 0.7 s for model C (IH).

Models A′, B′, and C′ differ from models A, B, and C, respectively, only in the overall normalization of the neutrino fluxes. Each model of the former set has the same best-fit value of t_{off} as its counterpart in the latter set because they have the same time profile of neutrino emission. On the other hand, although both the scale factor K and the distance d change the overall flux normalization, the neutrino fluxes corresponding to the best-fit values of K differ significantly from those corresponding to the best-fit values of d (equivalent to $K \approx 1$). These differences are caused by the different prior probabilities $p(K|M_i)$ and $p(d|M_i)$, with the former being much less restrictive than the latter. Likewise, the K values enclosed by the 95% credible regions for models A′, B′, and C′ correspond to much larger variations of the neutrino fluxes than the d values for models A, B, and C. The t_{off} values enclosed by the 95% credible regions, however, show few differences between the two sets of models.

Tables III and IV show that there is hardly any noticeable preference among the three cases of neutrino oscillations for each baseline model (A, B, or C) or its counterpart (A′, B′, or C′). With a Bayes factor $B_{ij} \approx 34$–65, model A is strongly preferred to model B regardless of neutrino oscillations. The evidence in favor of model A over model C, however, is hardly noticeable to positive with $B_{ij} \approx 2.2$–5.4. By comparison, model A′ is positively preferred to model B′ with $B_{ij} \approx 3.4$–11, while the evidence in favor of model A′ over model C′ is hardly noticeable to positive with $B_{ij} \approx 1.2$–4.4.

V. COMPATIBILITY OF BEST-FIT MODELS WITH DATA

While the Bayesian approach can provide parameter estimates and rank the models, it does not address the compatibility of the models with the data. To check the compatibility, we take the frequentist approach. Specifically, we apply this approach to test the compatibility of the best-fit models presented in Sec. IV with the SN 1987A data. For model M_i with the set of best-fit parameters $\boldsymbol{\theta}_{bf}$, the probability of detecting an event with energy E at time $t_{det} = t - t_{off}$ is given by $p(E, t|\boldsymbol{\theta}_{bf}, M_i)$ [see Eq. (8)]. Using this probability, we obtain the contours expected to enclose 68% and 95% of the events on the $t - E$ plane. These contours are shown in Figs. 4 and 5 for models A, B, C and A′, B′, C′, respectively, along with the data. It can be seen that for each model in the former set and its counterpart in the latter set, the comparison of the contours with the data is very close. In addition, for all the models, the contours are rather consistent with the data on the 11 events.

For a more formal check of the compatibility, we perform a p-value test (see, e.g., [22]), which can be viewed as a more technical version of the comparisons shown in Figs. 4 and 5. Because the comparison of the best-fit model with the data is very close for the two sets of models, we carry out the p-value tests for the best-fit models A′, B′, and C′ for illustration. We draw a total of $\mathcal{N}_{tot} = 10^6$ samples, each consisting of $N = 11$ events, from the probability distribution $p(E, t|\boldsymbol{\theta}_{bf}, M_i)$ and calculate the statistic
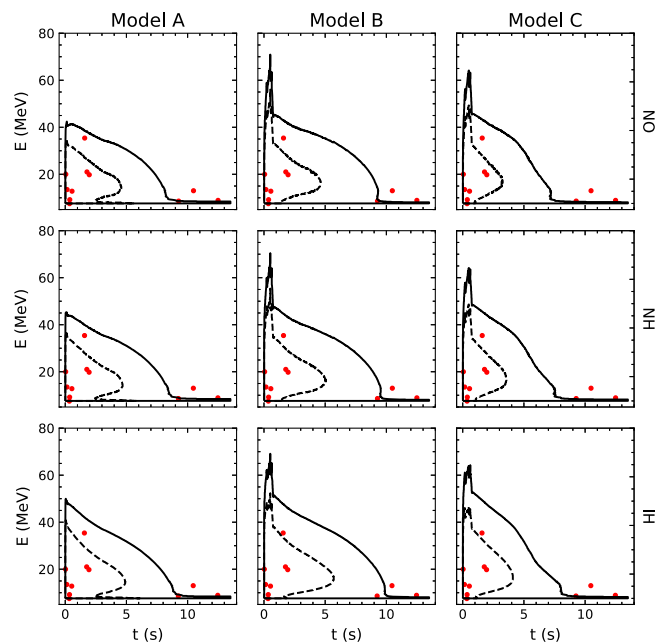

FIG. 4. The contours expected to enclose 68% (dashed curve) and 95% (solid curve) of the events for the best-fit models A, B, and C including three cases of neutrino oscillations are compared with the SN 1987A data (filled circles).
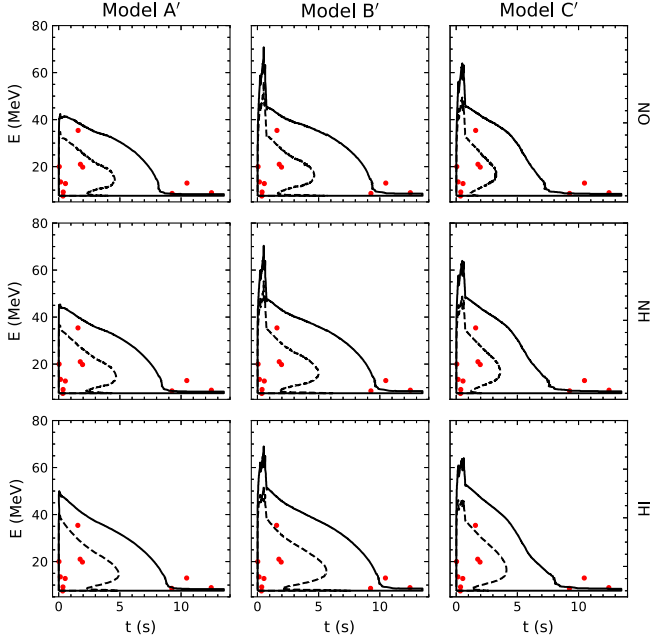
FIG. 5.   Same as Fig. 4, but for the best-fit models A′, B′, and C′.

$$\lambda = \prod_{j=1}^{N} p(E_j, t_j | \boldsymbol{\theta}_{\mathrm{bf}}, M_i) \qquad (16)$$

for each sample. The p value is $\mathcal{N}_{\mathrm{ex}}/\mathcal{N}_{\mathrm{tot}}$, where $\mathcal{N}_{\mathrm{ex}}$ is the number of extreme samples with $\lambda \le \lambda_{\mathrm{det}}$ and λ_{det} is the statistic calculated for the detected events. Histograms of the sample test statistics are shown in Fig. 6, and the p
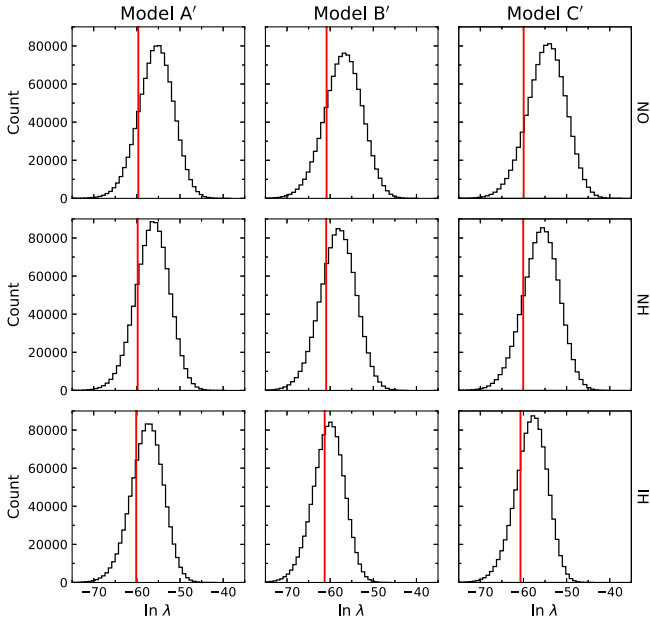

FIG. 6.   Histograms of the statistic $\ln\lambda$ are shown for samples of the best-fit models A′, B′, and C′ including three cases of neutrino oscillations. A total of 10^6 samples are simulated for each model. The red lines denote the corresponding values of $\ln\lambda$ for the SN 1987A data.

values for the best-fit models A′, B′, and C′ are given in Table IV. A p value smaller than 0.05 is usually taken as evidence for rejecting the corresponding model, while a p value exceeding 0.05 simply indicates no evidence that the model is incompatible with the data. Table IV shows that the test yields no evidence of inconsistency between the best-fit models A′, B′, and C′ and the SN 1987A data, as expected from the comparisons shown in Fig. 5.

VI. CONCLUSIONS

We have used the Bayesian approach to compare three baseline simulated models of SN neutrino emission (see Table I and Fig. 1) with the KII data on SN 1987A. Without any modification other than inclusion of possible effects of neutrino oscillations, we find that model A with a brief accretion phase and a total energy of $\mathcal{E}_\nu = 1.99 \times 10^{53}$ ergs emitted in all neutrino species is the most favored. Compared to model A, model B (C) with an extended accretion phase and $\mathcal{E}_\nu = 4.28 \times 10^{53}$ (3.30×10^{53}) ergs is strongly (barely to positively) disfavored. Allowing for variation of the overall neutrino flux normalization, we find that compared to model A′ with a brief accretion phase, model B′ (C′) with an extended accretion phase is positively (barely to positively) disfavored. The best-fit model A′ has $\mathcal{E}_\nu \approx (2.3\text{–}2.6) \times 10^{53}$ ergs depending on the case of neutrino oscillations, while the best-fit models B′ and C′ both have $\mathcal{E}_\nu \approx 2.0 \times 10^{53}$ ergs regardless of neutrino oscillations (see Table IV). All the best-fit models (A, B, C, and A′, B′, C′) have $\mathcal{E}_\nu$ consistent with the PNS gravitational binding energy, $\mathcal{E}_G \approx 1.34 \times 10^{53}(M_G/M_\odot)^2$ erg, which is $\sim(1.34\text{–}5.36) \times 10^{53}$ erg for a theoretically expected gravitational mass of $M_G \sim 1\text{–}2$ $M_\odot$ [23]. We also find no evidence that any of the best-fit models are incompatible with the data (see Figs. 4 and 5 and Table IV).

As presented here, even with only the eleven events observed in the KII detector, we are able to differentiate models of neutrino emission for SN 1987A. Our analyses can easily be extended to models not discussed here (e.g., [24]). A future SN in the Galaxy is expected to produce $\sim 10^4$ IBD events in the Super-Kamiokande detector (e.g., [25]). That many events would provide much better differentiation among models of neutrino emission for that SN. Comparing models with data at that level would provide an important test of our understanding of the relevant physics and help improve SN simulations.

[1] K. Hirata *et al.*, Observation of a Neutrino Burst from the Supernova SN1987A, Phys. Rev. Lett. **58,** 1490 (1987).

[2] K. S. Hirata *et al.*, Observation in the Kamiokande-II detector of the neutrino burst from supernova SN1987A, Phys. Rev. D **38,** 448 (1988).

[3] R. M. Bionta *et al.*, Observation of a Neutrino Burst in Coincidence with Supernova 1987A in the Large Magellanic Cloud, Phys. Rev. Lett. **58,** 1494 (1987).

[4] E. Alexeyev *et al.*, Detection of the neutrino signal from SN 1987A in the LMC using the INR Baksan underground scintillation telescope, Phys. Lett. B **205,** 209 (1988).

[5] W. D. Arnett, J. N. Bahcall, R. P. Kirshner, and S. E. Woosley, Supernova 1987A, Annu. Rev. Astron. Astrophys. **27,** 629 (1989).

[6] T. J. Loredo and D. Q. Lamb, Bayesian analysis of neutrinos observed from supernova SN 1987A, Phys. Rev. D **65,** 063002 (2002).

[7] M. L. Costantini, A. Ianni, G. Pagliaroli, and F. Vissani, Is there a problem with low energy SN1987A neutrinos? J. Cosmol. Astropart. Phys. 05 (2007) 014.

[8] H.-T. Janka, Explosion mechanisms of core-collapse supernovae, Annu. Rev. Nucl. Part. Sci. **62,** 407 (2012).

[9] A. Mirizzi, I. Tamborra, H.-T. Janka, N. Saviano, K. Scholberg, R. Bollig, L. Hudepohl, and S. Chakraborty, Supernova neutrinos: Production, oscillations and detection, Riv. Nuovo Cimento **39,** 1 (2016).

[10] https://wwwmpa.mpa-garching.mpg.de/ccsnarchive/.

[11] A. W. Steiner, M. Hempel, and T. Fischer, Core-collapse supernova equations of state based on neutron star observations, Astrophys. J. **774,** 17 (2013).

[12] J. M. Lattimer and D. F. Swesty, A generalized equation of state for hot, dense matter, Nucl. Phys. **A535,** 331 (1991).

[13] I. Tamborra, B. Mueller, L. Huedepohl, H.-T. Janka, and G. Raffelt, High-resolution supernova neutrino spectra represented by a simple fit, Phys. Rev. D **86,** 125031 (2012).

[14] N. Panagia, R. Gilmozzi, F. Macchetto, H. M. Adorf, and R. P. Kirshner, Properties of the SN 1987A circumstellar ring and the distance to the large magellanic cloud, Astrophys. J. **380,** L23 (1991).

[15] N. Panagia, A geometric determination of the distance to SN 1987A and the LMC, Springer Proc. Phys. **99,** 585 (2005).

[16] A. S. Dighe and A. Y. Smirnov, Identifying the neutrino mass spectrum from a supernova neutrino burst, Phys. Rev. D **62,** 033007 (2000).

[17] M. C. Gonzalez-Garcia, M. Maltoni, and T. Schwetz, Updated fit to three neutrino mixing: Status of leptonic *CP* violation, J. High Energy Phys. 11 (2014) 052.

[18] P. Zyla *et al.* (Particle Data Group), Review of particle physics, Prog. Theor. Exp. Phys. (**2020**), 083C01.

[19] B. Jegerlehner, F. Neubig, and G. Raffelt, Neutrino oscillations and the supernova 1987A signal, Phys. Rev. D **54,** 1194 (1996).

[20] C. Lunardini and A. Smirnov, Neutrinos from SN1987A: Flavor conversion and interpretation of results, Astropart. Phys. **21,** 703 (2004).

[21] R. Barlow, Extended maximum likelihood, Nucl. Instrum. Methods Phys. Res., Sect. A **297,** 496 (1990).

[22] C.-H. Li, Astrophysics and physics of neutrino detection, Ph.D. thesis, University of Minnesota, 2017.

[23] F. X. Timmes, S. E. Woosley, and T. A. Weaver, The neutron star and black hole initial mass function, Astrophys. J. **457,** 834 (1996).

[24] H. Nagakura, A. Burrows, and D. Vartanyan, Supernova neutrino signals based on long-term axisymmetric simulations, Mon. Not. R. Astron. Soc. **506,** 1462 (2021).

[25] K. Scholberg, Supernova neutrino detection, Annu. Rev. Nucl. Part. Sci. **62,** 81 (2012).